

# Climate Sensitivity Parameter in the Test of the Mount Pinatubo Eruption

Antero Ollila<sup>1\*</sup>

<sup>1</sup> Department of Civil and Environmental Engineering (Emer.), School of Engineering, Aalto University, Espoo, Finland  
Otakaari 1, Box 11000, 00076 AALTO, Finland

## ABSTRACT

The author has developed a dynamic model (DM) to simulate the surface temperature change ( $\Delta T$ ) caused by the eruption of Mount Pinatubo. The main objectives have been 1) to test the climate sensitivity parameter ( $\lambda$ ) values of  $0.27 \text{ K/(Wm}^{-2}\text{)}$  and  $0.5 \text{ K/(Wm}^{-2}\text{)}$ , 2) to test the time constants of a simple first-order dynamic model, and 3) to estimate and to test the downward longwave radiation anomaly ( $\Delta \text{LWDN}$ ). The simulations show that the calculated  $\Delta T$  of DM follows very accurately the real temperature change rate. This confirms that theoretically calculated time constants of earlier studies for the ocean (2.74 months) and for the land (1.04 months) are accurate and applicable in the dynamic analyses. The DM-predicted  $\Delta T$  values are close to the measured value, if the  $\lambda$ -value of  $0.27 \text{ K/(Wm}^{-2}\text{)}$  has been applied but the  $\lambda$ -value of  $0.5 \text{ K/(Wm}^{-2}\text{)}$  gives  $\Delta T$  values, which are about 100 % too large. The main uncertainty in the Mount Pinatubo analyses is the  $\Delta \text{LWDN}$  flux, because there are no direct measurements available during the eruption. The author has used the measured ERBS fluxes and has also estimated  $\Delta \text{LWDN}$  flux using the apparent transmission measurements. This estimate gives the best and most consistent results in the simulation. A simple analysis shows that two earlier simulations utilising General Circulation Models (GCM) by two research groups are depending on the flux value choices as well as the measured  $\Delta T$  choices. If the commonly used minimum value of  $-6 \text{ Wm}^{-2}$  would have been used for the shortwave anomaly in the GCM simulations, instead of  $-4 \text{ Wm}^{-2}$ , the  $\Delta T$  values would differ from the measured  $\Delta T$  values almost 100 %. The main reason for this error seems to be the  $\lambda$ -value of  $0.5 \text{ K/(Wm}^{-2}\text{)}$ .

*Keywords: Global warming, climate sensitivity parameter, climate response time, radiative forcing response, downward radiative fluxes, Mount Pinatubo eruption.*

## 1. INTRODUCTION

### 1.1 Objectives and Symbols

The Mount Pinatubo eruption in 1991 caused a global cooling during the next five years as the incoming shortwave radiation was reduced by  $6 \text{ W/m}^2$  offering a unique opportunity to test and to analyse the various phenomenon of the climate system. Water vapour feedback has remained a topic of debate since 1990 and the eruption can be used to analyse this effect also. The first objective of this paper is to test the two climate sensitivity parameter values which have been commonly used in the scientific studies. The second objective is to test the climate system time constants describing the dynamic behaviour of the climate exposed to a relative big and sudden change. The third objective is to estimate and to test

the downward longwave radiation anomaly ( $\Delta\text{LWDN}$ ). In the simulations a theoretical feedback property of the climate system has been also tested.

Table 1 includes all the symbols, abbreviations, acronyms and definitions used repeatedly in this paper.

**Table 1. List of symbols, abbreviations, and acronyms**

Acronym	Definition
<b>DM</b>	One dimensional dynamic model
AT	Apparent transmission
ENSO	El Niño Southern Oscillation
ERBS	NASA's Earth Radiation Budget Satellite
GCM	General Circulation Model
ISCCP	International Satellite Cloud Climatology Project
LW	Longwave
LWDN	LW radiation flux downward
LWUP	LW radiation flux upward
LWSRF	LW radiation emitted by the surface
OLR	Outgoing longwave radiation
ONI	Oceanic Niño Index
RF	Radiative forcing change
SW	Shortwave
SWATM	SW radiation flux absorbed by the atmosphere
SWIN	SW radiation flux incoming at the TOA
SWSRF	SW radiation flux incoming at the surface
TOA	Top of the atmosphere
TPW	Total precipitable water
T	Surface temperature
T <sub>m</sub>	1DM-predicted surface temperature change
T <sub>av</sub>	Average surface temperature change by four datasets
T <sub>msu</sub>	Surface temperature change by UAH MSU dataset
T <sub>av-e</sub>	T <sub>av</sub> with ENSO correction
T <sub>msu-e</sub>	T <sub>msu</sub> with ENSO correction
TCS	Transient climate sensitivity
$\lambda$	Climate sensitivity parameter
$\Delta$	Anomaly or change

Subscript<sub>n</sub> means step n in time domain.

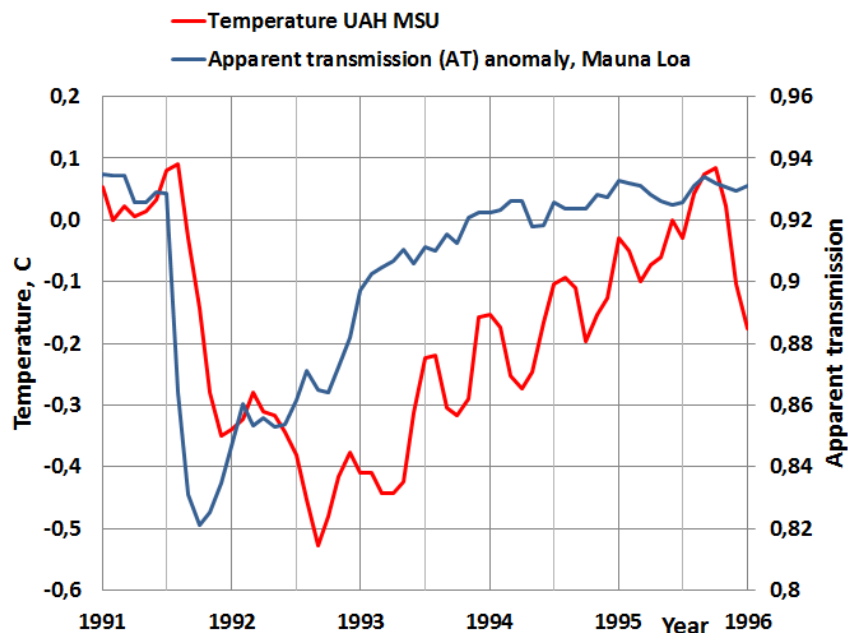
## 1.2 The Mount Pinatubo eruption

The main eruption of the Mount Pinatubo volcano (15.1 °N, 120.3 °E) on the island of Luzon in the Philippines began on the 3<sup>rd</sup> of June, 1991 and concluded on the next day. Four large explosions generated eruption columns reaching the heights of up to 24 km in the stratosphere. The estimate of the stratospheric mass increase was 14 – 20 Mt of SO<sub>2</sub>, which created 21-40 Mt of H<sub>2</sub>SO<sub>4</sub>–H<sub>2</sub>O aerosols [1]. The eruption also injected vast quantities of minerals and metals into the troposphere and stratosphere in the form of ash particles. The aerosols formed a global layer of sulfuric acid haze over the globe and the global temperatures dropped about 0.5 °C in the years 1991 – 1993.

The sulphate aerosols caused scattering of the visible light and therefore the incoming radiation scattered more effectively back into space. Thus the albedo of the Earth increased leading to a cooling at the Earth's surface. On the other hand the plants utilized the climate conditions, because they could photosynthesize more effectively in the diffuse sunlight [2]-

55 [3]. As a result of the more intensive photosynthesis, there was a negative anomaly of the  
56 global CO<sub>2</sub> concentration increase rate.

57 Because the eruption happened at one point, it took several weeks before the global effect  
58 was fully developed. The volcanic aerosol cloud encircled the Earth in 21 days driven by the  
59 easterly winds in the tropical stratosphere. It covered about 42 % of the Earth in two weeks  
60 [4]. In Fig. 1 are depicted the global temperature [5] and the apparent transmission  
61 measured at Mauna Loa [6] (19.3 °N, 155.4 °W). It can be seen that there is delay between  
62 the temperature response and the apparent transmission (AT) describing the reduction of  
63 the incoming shortwave (SW) radiation.



64

65 **Fig.1. The global satellite temperature and the apparent transmission measured at**  
66 **Mauna Loa, Hawaii.**

67 In Fig. 2 the apparent transmissions (AT) are depicted at the various sites on the northern  
68 hemisphere [7]. It can be seen that the absolute values of the AT values are different  
69 depending mainly on the local conditions. For example, the low values of the Japanese sites  
70 describe the air quality of the local conditions. The large value of the Mauna Loa is due to  
71 the fact that it is at the altitude of 3.4 km in the middle of the Pacific. An important feature  
72 thinking the analysis methods of this study is that the percentage decreases are very close  
73 to each other in the range from 10.1 % to 13.2 %.

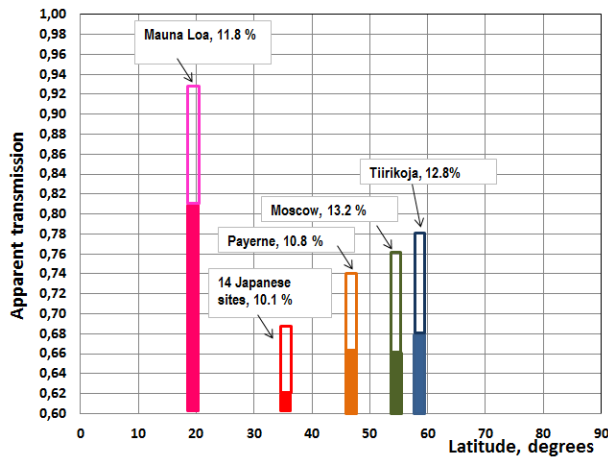


**Fig. 2. The apparent transmission values at the various sites. The percentage values show the maximum decreases of the apparent transmissions after the eruption and they are represented by light bars inside the normal apparent values (total bar length).**

The sites in Fig. 2 cover almost 85 % of the northern hemisphere. Thomas [8] has analyzed the global apparent transmission measurements after the eruption. The analysis shows that the aerosol cloud was covering the latitudes from 60S to 60N after three months and practically uniform over the hemispheres after six months. This is also the moment of the maximum temperature decrease. The main role in spreading the cloud had planetary scale waves in high latitudes, which transported the volcanic aerosol from the tropics to high latitudes. The reason why the decrease of apparent transmission value was almost the same at the high latitudes as in the tropics is probably due to the zenith angle. Even though the sulphate cloud would be thinner at the high latitudes, the sunlight has a longer pathway through the atmosphere. **This phenomenon can compensate the effects of possible thinner cloud conditions.**

Two conclusions can be drawn from these figures. The global delay called a dead time in process dynamics, is estimated to be 1.6 months between the incoming SW radiation change and the global surface temperature response. This value is used in the dynamical analyses of this study.

Another conclusion is that after the fully developed coverage of the sulphate cloud in the stratosphere, the radiation effect changes can be estimated to happen simultaneously over the globe. Therefore it is justified to use the one dimensional (1D) approach in developing a dynamic model (called **DM**) for analysing the temperature versus radiation flux relationships.

### 1.3 Literature study

There have been numerous Pinatubo studies on the three major fields. The first is on the aerosol and chemical effects of the Pinatubo particles. The second is focused on optical properties of the aerosol particles and on the radiative forcing. The third is on the responses to the forcing affecting the temperature and the circulation patterns.

This paper concentrates on the dynamic behaviour of the surface temperature changes caused by the radiative flux changes. Therefore the survey of the earlier studies covers only the subjects which are relevant for this study.

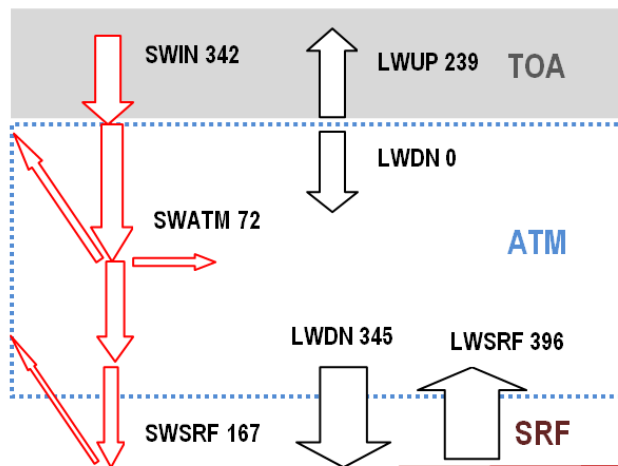
Even though the Pinatubo eruption is the best documented major eruption so far, there was

an essential radiative flux, which was not directly measured during the eruption. This was the LW downward radiation flux (LWDN), which is essential, because it compensates the major portion of the cooling effects of the reduced SW downward radiation flux (SWIN) decrease during the early phases of the eruption [9].

The World Climate Research Programme (WCRP) Radiative Fluxes Working Group initiated a new Baseline Surface Radiation Network (BSRN) to support the research projects. Some years later the BSRN was incorporated into the WCRP Global Energy and Water Cycle Experiment (GEWEX). The BSRN network stations started to operate in 1992 and that is why these valuable measurements were not available during the Pinatubo eruption.

There has been a special GEWEX project to assess the surface radiation budget datasets [10] based on the available data at the top of the atmosphere (TOA). By studying the GEWEX results, the author's conclusion is that the LWDN fluxes could not be estimated reliably in this project based on the other existing flux data. Therefore a major challenge in this study is to estimate the  $\Delta$ LWDN flux trend during the Pinatubo eruption.

In Fig. 3 the main radiative fluxes of the Earth are illustrated [11]-[12]. The climate forcing effect of a volcano eruption can be analysed in the same way as the cloud change forcing. Normally the cloud forcing has been calculated as the sum of changes in the downward SW flux change and outgoing LW flux change between the clear and all-sky conditions. Applying this same method, the radiative forcing (RF) caused by the eruption, is the sum of  $\Delta$ SWIN and  $\Delta$ LWUP and it is called aerosol radiative forcing [13]. The change in the flux values is calculated between the normal conditions and during or after the eruption. Because the outgoing LW flux is reduced during the early phases of the eruption, it is a sign that there is cooling happening on the surface.



140  
141

142 **Fig. 3. The main radiative fluxes of the Earth's energy balance.**

143

144 The RF value calculated in this way is normally called radiative or climate forcing (RF).  
 145 Actually it is only a measure of the real RF. There are two fluxes which have the real forcing  
 146 effect on the Earth's surface temperature (T) and they are SWIN and LWDN. They are the  
 147 only fluxes, which form the radiation input on the surface. In the change from the all-sky to  
 148 the cloudy sky conditions, the change of LWUP at the TOA is  $-11 \text{ Wm}^{-2}$  and the change of  
 149 LWDN at the surface is  $+14.3 \text{ Wm}^{-2}$  [12]. These flux values show that if the clear sky  
 150 conditions do not prevail, the LWUP change is not equal to the real warming/cooling impact  
 151 on the surface caused by the LWDN flux change. This example also shows that the LWDN

flux change is greater than the LWUP flux change. The major reason for this difference is that the cloudy sky values are actually measured in the dynamic situation and the LWUP flux is not in the real equilibrium value.

The small particle sizes less than 1  $\mu\text{m}$  are more effective in reflecting the SW solar radiation SWIN than they are at reflecting the LW radiation emitted by the surface. According to a comprehensive study [1], the smallest particles were sulphuric acid/water droplets and the largest particles were ash fragments. The cooling and warming effects of the aerosols and particles depend on the particle sizes. The LWDN flux increases especially during the early phases of the eruption because there are larger aerosol particles more in the atmosphere than in the later phases. Therefore the warming effect of LWDN is the most effective at the same time as the cooling is in maximum [1],[9]. The stratospheric ash layer settled down just above the troposphere staying there until March 1992. The particle size measurements [1],[4] showed that there was a peak in both small and large particle sizes after a few months after the eruption but by 1993 the high measurements values were decaying back to pre-eruption values.

The ash cloud in the high altitudes of the atmosphere absorbs and emits radiation. This ash cloud had a measureable warming effect on the northern hemisphere winter temperatures [14]-[15]. The ash cloud has about the same effect as the clouds have in the cold climate conditions, it will prevent the cooling of the surface. In this way it has a net warming effect.

The radiative forcing (RF) at TOA has a linear relationship to the global mean surface temperature change  $\Delta T$ , if the equilibrium state is assumed [16]:

$$\Delta T = \lambda \text{RF}, \quad (1)$$

where  $\lambda$  is the climate sensitivity parameter, which is a nearly invariant parameter having a value of 0.5 K/(Wm<sup>-2</sup>). IPCC uses still equation (1) in its latest report AR5 but IPCC no longer keeps the value of  $\lambda$  almost constant [17]. A general experience and also a common practice is to approximate the small changes around the operating point to be linear by nature. The most probable change of RF by the end of this century is 6 Wm<sup>-2</sup> according to RCP6 (Representative Concentration Pathways) [17]. This change is only 2.5 % about the average value of OLR (outgoing longwave radiation) value of 239 Wm<sup>-2</sup>.

The author carried out a study about this issue utilizing the MODTRAN code [18]. The concentration of CO<sub>2</sub> varied from 357 ppm to 700 ppm and the sky conditions were clear and cloudy, which were combined to calculate the all-sky values. The average global atmosphere profiles for GH gases, temperature and pressure were applied. The results show that the maximum nonlinearity between the OLR fluxes was 0.01 % and the maximum variation in  $\lambda$  values was 2.5 %, when the surface temperature varied  $\pm 1$  °C. These results show that the equation (1) is applicable for small RF and temperature changes.

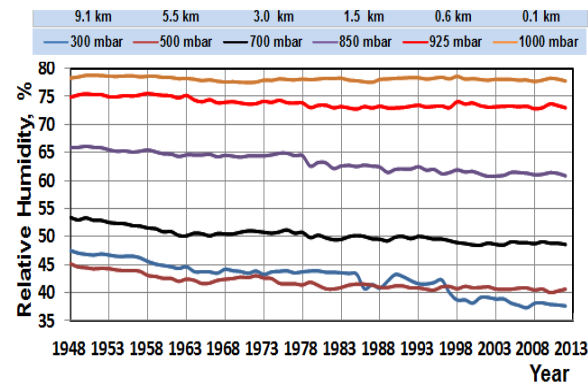
Ollila has analysed [19] the future warming values based on the RF values of greenhouse gases. This analysis showed that the warming values of RCP2.5, RCP4.5, and RCP6 could be calculated using the  $\lambda$  value of  $\sim 0.37$  K/(Wm<sup>-2</sup>). IPCC has calculated RCP warming values applying GCMs but they do not inform the possible  $\lambda$  values. On the other hand IPCC reports in AR5 [17] that the transient climate sensitivity (TCS) value is likely to lie in the range 1 to 2.5 °C giving the average value 1.75 °C. This value is almost the same as calculated by equation (1):  $\Delta T = 0.5 \text{ K/(Wm}^{-2}) * 3.7 \text{ Wm}^{-2} = 1.85 \text{ K}$ . The conclusion is that IPCC is very inconsistent in using  $\lambda$  values and equation (1). If  $\lambda$  is not “nearly invariant parameter”, IPCC should have introduced something more credible scientific evidence about the real nature of  $\lambda$ .

205  
206  
207  
208  
209  
210  
211  
212  
213  
214  
215  
216  
217  
218  
219  
220  
221  
222  
223  
224  
225  
226  
227  
228  
229  
230  
231  
232

This inconsistency may be linked to the warming values of the recent RF values. There should not be any of IPCC's own climate models, but in reality there is such a model called "Radiative Forcing by Emissions and Drivers" which has a summary leading to the value of  $2.34 \text{ Wm}^{-2}$  according to AR5 [17]. IPCC denies that there is any IPCC's model but the fact is that the IPCC organization has selected a number of research studies, which have been used in creating their presentation. There are private researchers who do not make the same selections and therefore their models are different. If equation (1) is applied in the same way as calculating the TCS value above, the warming value of  $2.34 \text{ Wm}^{-2}$  would be  $1.17^\circ\text{C}$  in 2011. IPCC does not show this temperature increase in the AR5 [17], and one reason might be that it is 38 % greater than the observed value of  $0.85^\circ\text{C}$ .

The possible water feedback is the only essential feedback in TCS calculations. In the referred GCM studies applied in the Pinatubo analyses, there are no reported  $\lambda$  values. The lambda value of  $0.5 \text{ K/(Wm}^{-2})$  means that there is a positive water feedback included into a model. The assumption that there is a positive water feedback in the climate models means that relative humidity (RH) should be constant despite the moderate warming/cooling of the atmosphere. This property of the positive water feedback would double the warming effects of GH gases according to AR4 [16]. IPCC reports in AR5 that the positive water feedback can amplify any forcing by a typical factor between two and three [17]. This means that understanding of water feedback magnitude is not becoming more accurate but it has become more inaccurate.

The issue of a constant RH can be studied by simply looking at the RH trends since 1948, which are depicted in Fig. 4 [20]. It is clear that RH has varied quite a lot. Even though the early RH measurements may be unreliable, the measurements since 1980 have better technology and they are very accurate and reliable.



233  
234  
235  
236  
237

**Fig. 4. The global relative humidity trends according to NOAA at different altitudes in the troposphere.**

238  
239  
240  
241  
242  
243  
244  
245  
246

The positive water feedback and high climate sensitivity (CS) of climate models is a well-known feature. Normally the equilibrium CS varies from  $1.5^\circ\text{C}$  to  $4.5^\circ\text{C}$  [21], which means that the variation of TCS (Transient climate sensitivity) is about half of this range. However there are several studies, which have calculated the climate sensitivity value to be about  $1.0 - 1.2^\circ\text{C}$  [22]-[25] using the same radiative forcing value of  $3.7 \text{ Wm}^{-2}$  for  $\text{CO}_2$  as IPCC uses. It means a lower  $\lambda$  value of about  $0.27 - 0.3 \text{ K/(Wm}^{-2})$ . Some researchers have calculated even lower values like  $\sim 0.6^\circ\text{C}$  for climate sensitivity [19], [26] or  $0.7^\circ\text{C}$  [27]. Ollila [19] has calculated the  $\lambda$  value using three different methods and his results vary between 0.245 and 0.331 the most reliable value being  $0.268 \text{ K/(Wm}^{-2})$ . In this study these two most common



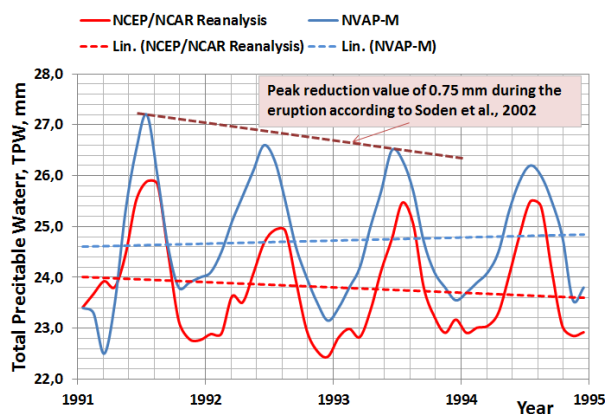
247 values have been applied:  $0.27 \text{ K}/(\text{Wm}^{-2})$  and  $0.5 \text{ K}/(\text{Wm}^{-2})$ .  
248

249 The forcing studies can be classified into two categories namely forcing calculations utilising  
250 General Circulation Models (GCM) 1) for simulations of spatial flux and temperature changes  
251 [8], [28]-[31], and 2) other simulations resulting the surface temperature change. In respect  
252 to this study only the latter studies are relevant.  
253

254 One of the earliest studies was that of Hansen et al. [32]. They used the GISS global climate  
255 model to assess the preliminary impacts of the Pinatubo eruption. In their calculations they  
256 used the peak value of  $-4 \text{ Wm}^{-2}$  for  $\Delta\text{SWIN}$  and they could show that the simulated  $\Delta T$  was  
257 about  $-0.5 \text{ }^{\circ}\text{C}$ . The most common value of  $\Delta\text{SWIN}$  has been  $-6 \text{ Wm}^{-2}$  [8], [13]-[14], [29], [33].  
258 This value is also used in this study.  
259

260 In the later study [34] Hansen et al. applied the same peak value of  $-4 \text{ Wm}^{-2}$  in the GCM  
261 simulations by name SI94 and GRL92. Soden et al. [35] applied a GCM and as input data  
262 they used ERBS fluxes in calculating the RF values. They also included the absolute  
263 atmospheric water content as a variable. The peak value of  $-4 \text{ Wm}^{-2}$  was used for  $\Delta\text{SWIN}$ .  
264 Their major result was the GCM simulations could calculate the  $\Delta T_m$  values close to the  
265 measured value, if the positive water feedback was included. The water content was  
266 calculated using the NASA Water Vapor Project (NVAP) values [36].  
267

268 In Fig. 5 the NVAP dataset values as well the NCEP/NCAR (National Center for  
269 Environmental Prediction / National Center for Atmospheric Research) values are depicted  
270 [37]. The NVAP water content trends show great seasonal changes of about 3 TPW mm.  
271 Soden et al. [35] have reported that there has been  $\sim 0.75 \text{ TPW mm}$  peak reduction during  
272 the Pinatubo eruption. The graphs show that the peak reduction estimate [23] can be  
273 regarded a correct estimate. This choice of using the peak values only can be questioned,  
274 because the trend line of NVAP-M values show increased rate of absolute water content. A  
275 justified procedure would be to use the monthly values but then the water feedback effects  
276 would be huge. Because the seasonal water content variations depend mainly on the  
277 northern hemisphere seasonal changes, a better method might be to combine zonal  
278 temperature and water content values.  
279



280  
281 **Fig. 5. The graphs of water contents according to NVAP-M and NCEP/NCAR datasets.**  
282

283 In Fig. 5 it can be noticed that there are opposite trends in these datasets during the  
284 Pinatubo eruption. It is quite impossible to know, which of these datasets is correct and  
285 therefore the question of positive or negative water feedback cannot be reliably tested  
286 utilising the Pinatubo case and the global water content trends.  
287



## 2. RADIATIVE FLUXES AND FORCING ANOMALIES CAUSED BY THE ERUPTION

The two SWIN flux datasets available during the eruption are ISCCP [38] and ERBS [39]. They are depicted in Fig. 6. Both datasets are unstable and spiky. The SWIN flux anomaly can also be estimated using the apparent transmission (AT) signal or optical depth measurements. In this case the AT signal of Mauna Loa has been used. The  $\Delta$ SWIN flux anomaly has been assumed to follow exactly the trend of the AT-signal. The time of the minimum value of the AT-signal has been used to be also the time of the minimum value of the SWIN flux value of  $-6 \text{ Wm}^{-2}$ . This estimate of  $\Delta$ SWIN flux is depicted in Fig. 6 and it can be noticed that this flux is very stable and its trend follows very well the average form of ISCCP and ERBS fluxes. The smoothed  $\Delta$ ERBS SWIN flux signal follows the estimated AT transformed  $\Delta$ SWIN flux signal so well that they could be used between each other.

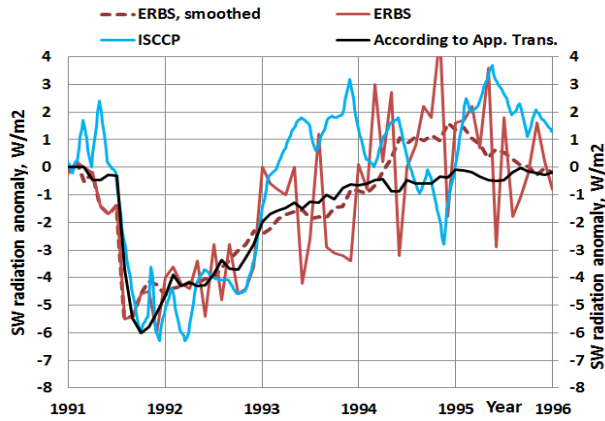


**Fig. 6. SW downward radiation flux anomalies at TOA.**

Because there are no direct measurements of LWDN flux, it has been estimated. As realized before, the LWDN flux anomaly should follow the amount of large aerosol particle amounts in the atmosphere. Russell et al. has a Fig. 6 in their paper [1] containing optical depth measurements of the different particle size trends measured at Mauna Loa during the eruption.

It has been assumed that the smaller particle sizes from  $0.382$  to  $0.500 \mu\text{m}$  are related to the  $\Delta$ SWIN flux anomaly. The largest particle size is  $1.020 \mu\text{m}$  and the graph of its aerosol optical depth has been used to estimate the  $\Delta$ LWDN flux. The peak values relationship between the  $1.020 \mu\text{m}$  and  $0.382/0.500 \mu\text{m}$  is  $0.6$ . Using this relationship the peak value of estimated  $\Delta$ LWDN flux anomaly would be  $0.6 * (-6 \text{ Wm}^{-2}) = -3.6 \text{ Wm}^{-2}$ . The  $\Delta$ LWDN is been estimated to follow the aerosol optical depth signal of the particle size  $1.020 \mu\text{m}$  at Mauna Loa and it is depicted in Fig. 7.

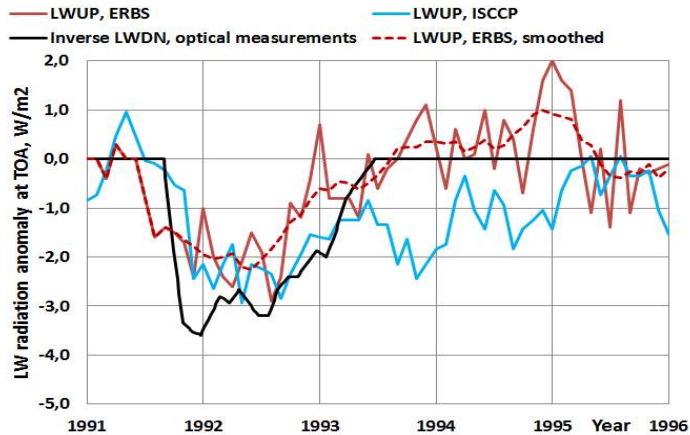


**Fig. 7. LW radiation flux anomalies at TOA.**

In Fig. 7 it can be noticed that the peak value of estimated LWDN flux is greater than the  $\Delta$ LWUP values measured at TOA by ISCCP and by ERBS. One explanation is that  $\Delta$ LWUP fluxes depend mainly on the surface temperature and therefore there is a dynamic delay in comparison to the  $\Delta$ LWDN flux. The full effect of this delay is about one year. In the dynamic situations like this Pinatubo eruption anomaly, the maximum temperature anomaly is about from 80% to 90 % from the full effect. This difference is analyzed more deeply in the simulation section.

In the simulations the measured surface temperature anomaly  $\Delta T$  is a reference. There are five dataset commonly available and four of them are depicted in Fig. 8 [5], [40]-[42]. There are rather big differences in the trends. The difference between the HadCRT4 and the UAH MSU, which is a lower atmosphere temperature measured by satellites, is even 0.4 °C around the beginning of the years 1992 and 1993. The UAH MSU trend has the largest minimum value during the eruption. Because of this situation, two surface temperature trends have been used as references namely Tmsu (UAH MSU dataset) and Tav (average of all four datasets).

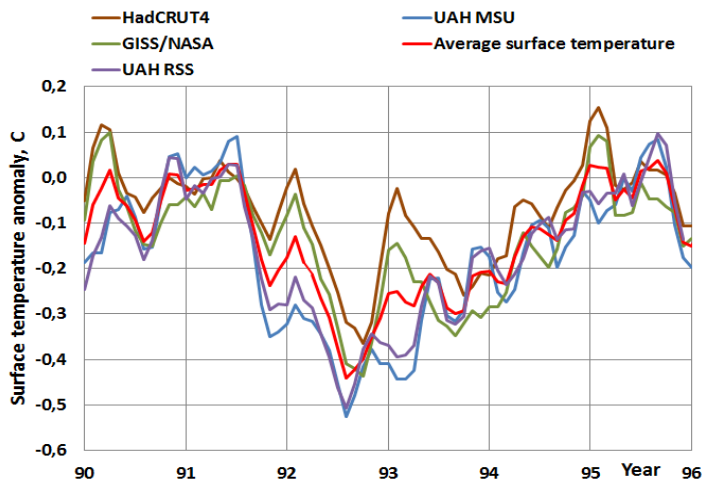
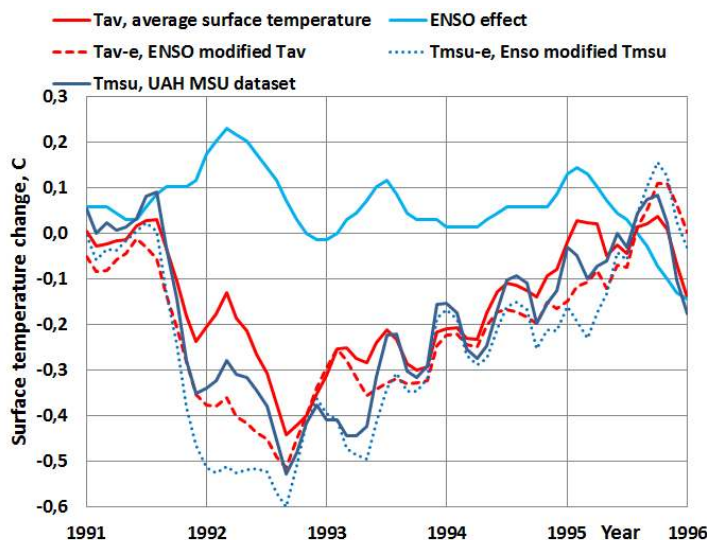


**Fig. 8. Surface temperature anomalies according to four datasets.**

343 Hansen et al. [34] and Soden et al. [35] have taken into account that the ENSO (El Niño  
 344 Southern Oscillation) phenomenon had the maximum warming index in January 1992, when  
 345 the Pinatubo eruption had the strongest cooling effects. The researchers eliminated the ENSO  
 346 effect by calculating a modified surface temperature of MSU UAH dataset. According to the  
 347 graphs of these two papers, the ENSO corrected minimum peak of  $\Delta T$  has been from -0.7  
 348 °C to -0.75 °C. They refer to the study of Santer et al. [43]. The author reads this same  
 349 paper that the maximum mean volcanically induced cooling  $\Delta T_{\max}$  at the surface is from  
 350 -0.35 °C to -0.45 °C and it is about double in the troposphere. ENSO certainly has a  
 351 warming effect from 1991 to the end of 1992, and therefore this result is not logical, because  
 352 the temperatures without ENSO corrections are about the same. There is a graph [43],  
 353 where the temperature anomaly is about -0.75 °C but it is for the troposphere and not for the  
 354 surface. Another study of Thompson et al. [44] shows that the maximum warming effect of  
 355 ENSO is only 0.14 °C.

357 Because the **quantified** effects of ENSO are so controversial, this study has used the results  
 358 of the own analyses. The elimination of ENSO is based on the analysis of ONI values  
 359 (Oceanic Niño Index) [45] and the global  $\Delta T$  values. The ENSO effect creates fluctuations,  
 360 which can be identified as almost identical fluctuations of  $\Delta T$  values after 1-12 months delay.  
 361 The four most regular El Niño / La Niña cases were selected. The relationship from peak to  
 362 peak between these fluctuations show that  $\Delta T = 0.144 * \Delta ONI$  on average. This temperature  
 363 effect formula has been used in modifying the measured  $\Delta T$  values but there is no time  
 364 delay applied, because the peak values of ONI and  $\Delta T$  values match. In Fig. 9 is depicted  
 365 the ENSO effect as a temperature anomaly and its effect on the two global  $\Delta T$  trends. This  
 366 approach gives the maximum ENSO effect of ~0.23 °C. The ENSO during the Pinatubo  
 367 eruption has a special feature not having the negative La Niña temperature peak at all.



369  
 370 **Fig. 9. The ENSO signal removed from the surface temperature measurement.**  
 371

372 The ENSO effect explains quite well why there is a peak upward from January 1992 to July  
 373 1992, when the surface temperature should be in minimum because of forcing by  
 374  $\Delta SWIN/\Delta LWDN$  anomaly. After 1993 the ENSO effect is very small, but it caused an upward  
 375 tick at the end of 1995, when the Pinatubo event was practically over. The ENSO modified  
 376 surface temperatures Tav-e and Tmsu-e have been used as references in this study.

### 3. DYNAMIC MODEL SIMULATIONS

The Pinatubo eruption happened in such a way that the forcing factors in the form of  $\Delta SWIN$  and  $\Delta LWDN$  flux anomalies changed all the time and therefore the applied model must be dynamical. A dynamical model is capable of simulating time dependent variables and their impacts. In this case a simple **dynamical model DM** has been applied as described in Fig. 10.

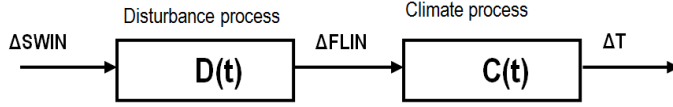


**Fig. 10. The dynamic simulation model of the climate system.**

The output  $\Delta FLIN$  of the disturbance process **D(t)** is the difference of  $\Delta SWIN$  and  $\Delta LWDN$  created by the Pinatubo eruption.  $\Delta FLIN$  has been delayed by 1.6 months **called dead time in process dynamics** and it can be formulated as follows:

$$\Delta FLIN = \Delta SWIN(t - \tau_D) - \Delta LWDN(t - \tau_D) \quad (2)$$

where  $t$  is time and  $\tau_D$  is dead time. The input variable  $\Delta SWIN$  is a flux anomaly signal varying according to the time as depicted in Fig. 6. Also  $\Delta LWDN$  varies according to the time as depicted in Fig. 7. The climate process **C(t)** includes two elements: 1) the input signal  $\Delta FLIN$  is transformed into the surface temperature change and 2) the dynamic behaviors of the climate system delays according two parallel first order transfer systems are included into  $\Delta T$  effects:

$$\Delta T = \lambda * \Delta FLIN * (K_{sea} * \exp(-t/T_{sea}) + K_{land} * \exp(-t/T_{land})) \quad (3)$$

where  $t$  is time (months),  $\exp$  is exponent,  $K_{sea}$  is 0.7,  $K_{land}$  is 0.3,  $T_{sea}$  is a time constant of 2.74 months and  $T_{land}$  is a time constant of 1.04 months. These values are based on the earlier studies [12], [46]-[47]. The values of the  $K$  parameters are the area portions of land and ocean of the Earth. The climate process **C(t)** is a combination of two parallel processes, because the time delays of land and ocean are different.

Three different simulation cases have been described and carried out: 1)  $\Delta SWIN$  and  $\Delta LWUP$  (the proxy of the  $LWDN$ ) fluxes are from ERBS datasets, 2)  $\Delta SWIN$  and  $\Delta LWDN$  are estimated as described above based on the AT measurements, 3) Feedback process experiment. The ISCCP dataset turned out to be too swaying and unreliable and therefore it has not been used. In cases 1) and 2) the simulations have been carried out by  $\lambda$  values of 0.27 K/(Wm<sup>-2</sup>) and 0.5 K/(Wm<sup>-2</sup>).

The dynamic processes according to eq. (2) are first-order dynamic models, which can be simulated in the discrete form enabling continuously changing input variables:

$$Out(n) = (\Delta t / (T + \Delta t)) * ((T / \Delta t) * (Out(n-1) + In(n))), \quad (4)$$

where  $Out(n)$  is the output of the process in step  $n$ ,  $In(n)$  is the input of the process of step  $n$ ,  $T$  is the time constant,  $\Delta t$  is the simulation step interval (=0.2 months), and  $n-1$  is the previous step value.

The results of using ERBS flux values are depicted in Fig. 11.

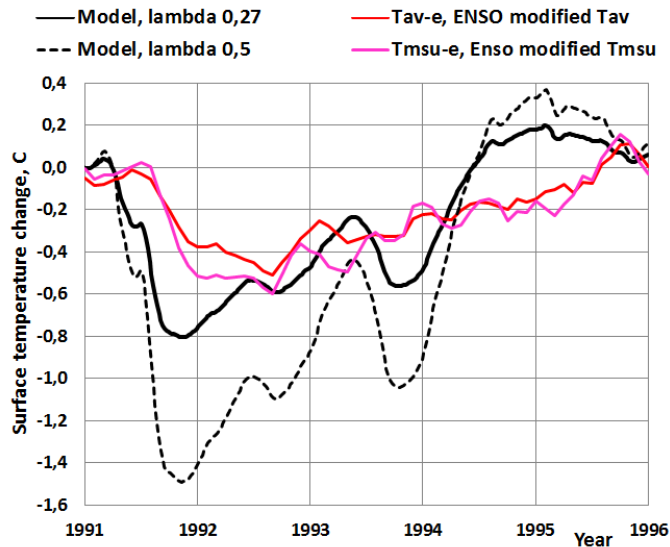


**Fig. 11. The simulated surface temperature according to the dynamic DM using ERBS dataset  $\Delta$ SWIN and  $\Delta$ LWUP fluxes.**

It can be noticed that the simulated temperature values vary a lot because the fluxes  $\Delta$ SWIN and  $\Delta$ LWIN vary too much. Especially the  $\lambda$  value of  $0.5 \text{ K/(Wm}^{-2}\text{)}$  gives  $\Delta T_m$  peak values, which are almost double as large as the  $\Delta T_m$  values using the  $\lambda$  value of  $0.27 \text{ K/(Wm}^{-2}\text{)}$ . A possible reason for this is that the LWUP flux anomaly is not an accurate enough estimate of the real  $\Delta$ LWDN flux anomaly and the flux measurements are too inaccurate.

In Fig. 12 the same graphs are depicted, when the  $\Delta$ SWIN and  $\Delta$ LWDN are estimated according to the AT and aerosol optical depth measurements. The simulated  $\Delta T_m$  signal is stable and the dynamic changes follow very well the real temperature changes  $\Delta T$ . Also in this case the  $\lambda$  value of  $0.5 \text{ K/(Wm}^{-2}\text{)}$  gives results, which do not follow the real changes of the surface temperature changes but gives about 100 % too great  $\Delta T_m$  during the eruption.

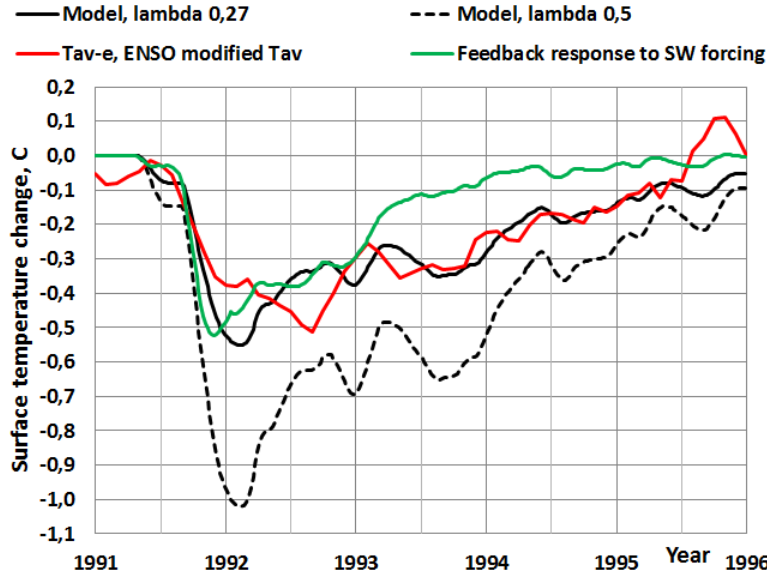


**Fig. 12. The simulated surface temperature according to the dynamic model using estimated SWIN and LWDN fluxes.**

The question of feedback has created the two schools of thoughts. Some researchers think that the climate system is like the other processes of the nature, which are built on negative feedbacks. A positive feedback system is dangerous, because it drives any system out of balance sooner or later. IPCC and some other researchers think that the climate system for example includes the positive water feedback as well as positive albedo and cloud feedbacks [17]. It should be noticed that the positive water feedback is included into the climate feedback parameter  $\lambda$ , when its value is  $0.5 \text{ K/(Wm}^{-2})$  [16] and should results in a constant RH trend in the troposphere. The  $\lambda$ -value of  $0.27 \text{ K/(Wm}^{-2})$  means a constant water content of the atmosphere.

A theoretical feedback process is simulated using the process model depicted in Fig. 13.

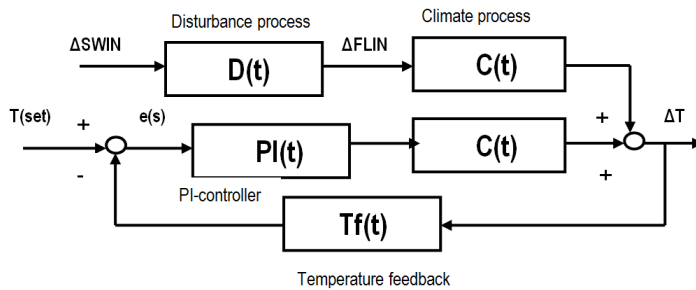


**Fig. 13. A theoretical feedback process in the case of Pinatubo eruption.**

The theoretical feedback process can be constructed based on the assumption that the  $\Delta\text{SWIN}$  flux anomaly is the only disturbance in a very stable climate system, which tries to eliminate this disturbance. The elimination process is a theoretical PI-controller, which detects a change in the surface temperature and creates an eliminating phenomenon, which tries to minimize the disturbance. In this case the eliminating flux is the  $\Delta\text{LWDN}$  flux. The climate process  $C(s)$  has as an input only the  $\Delta\text{SWIN}$  anomaly. The PI-controller imitates the



469 counter effect of  $\Delta\text{LWDN}$  flux but  $\Delta\text{LWDN}$  flux values are not needed to use in this  
470 simulation.

471

472 The mathematical form of the PI-controller (Proportional-Integral) in time domain is

473

474 
$$\text{Out}(t) = K_p * e(t) + (1/T_i) * \int e(t) dt \quad (5)$$

475

476 Where  $K_p$  is the gain of the controller,  $T_i$  is the integral time and  $e(t)$  is the error signal  
477 between the set point and the measurement. The equation (4) simulated in a discrete form in  
478 the time domain is

479

480 
$$\text{Out}(t) = K_p * \Delta e(t) + (K_p/T_i) \Sigma e(t) \Delta t \quad (6)$$

481

482 The PI-controller was tuned by trial and error giving  $K_p = 2$  and  $T_i = 500$  months. The results  
483 of the negative feedback process simulation are depicted in Fig. 12. The output of the  
484 theoretical feedback process follows the  $\Delta T_m$  values of DM surprisingly closely up to the end  
485 of 1993 as well as the measured  $\Delta T$  values.

486

487 One big difference between this study and the three referred studies [32], [35], and [36] is  
488 the use of estimated  $\Delta\text{LWDN}$  instead of measured  $\Delta\text{LWUP}$  fluxes. The basic reason is that  
489 these two fluxes have different values. The measured  $\Delta\text{LWUP}$  fluxes are not stable, making  
490 the results very unstable too. This problem can be eliminated to a certain degree by heavy  
491 smoothing or even by removing parts of a flux signal [35].

492

493 The actual  $\Delta\text{LWUP}$  flux depends on the surface temperature changes  $\Delta T$  which is caused by  
494 the RF change. The RF is the sum of  $\Delta\text{SWIN} + \Delta\text{LWDN}$  flux changes. The  $\Delta\text{LWUP}$  flux can  
495 be calculated using the measured  $\Delta T$  changes. The author has used two calculation  
496 methods. The first is MODTRAN radiation code available through Internet [18]. By applying  
497 the average global atmosphere profile, MODTRAN can calculate the LWUP flux change at  
498 TOA. The main parameters selected for these calculations were:  $\text{CO}_2$  357 ppm, fixed water  
499 vapor pressure, cloudy sky with cumulus cloud base of 0.66 km and top of 2.7 km. The 1 °C  
500 change in the surface temperature gives  $\Delta\text{LWUP}$  change of  $3.39 \text{ Wm}^{-2}$  for the clear sky and  
501  $3.08 \text{ Wm}^{-2}$  for the cloudy sky at TOA. By combining the two sky conditions, the all-sky value  
502 of 3.18 can be calculated [10]. Ollila [10] has calculated the same relationship using another  
503 commercial spectral analysis tool Spectral Calculator for the clear sky conditions. The cloudy  
504 sky fluxes are estimated to be 25 % less than the clear sky fluxes [16]. This calculation  
505 method gives the  $\Delta\text{LWUP}$  change of  $3.05 \text{ Wm}^{-2}$  for the 1 °C change. The results of  
506 MODTRAN calculation have been used, which gives a linear relationship

507

508 
$$\Delta\text{LWUP} = 3.18 * \Delta T. \quad (7)$$

509

510 This linear relationship is applicable inside the small temperature change of 1 °C.

511

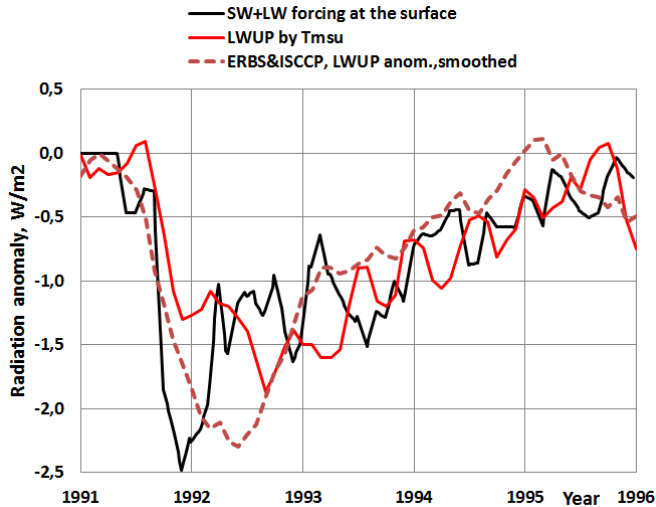


**Fig. 14. The LW fluxes during the Pinatubo eruption.**

The surface temperature calculated  $\Delta LWUP$  is depicted in Fig. 14. It can be compared to the measured  $\Delta LWUP$  flux, which is in this case the average of ISCCP and ERBS datasets. The flux values are at about the same level except for the first months of 1992. The SW+LW forcing flux is about  $1 \text{ Wm}^{-2}$  higher than the ISCCP & ERBE flux during the period 3/1992 – 10/1992. This could be due to the error of LWDN flux estimate. The LWDN flux may reduce quicker than the optical depth measurement indicates. This is also a probable reason for the difference between the  $T_m$  value of **DM** and the measurement based temperature anomalies during the year 1992. This is a very good result showing that  $\Delta LWUP$  depends on  $\Delta SWIN + \Delta LWDN$  fluxes and their dynamic effects on the  $\Delta T$  at the Earth's surface. Therefore,  $\Delta LWUP$  is not really the right choice in calculating the surface temperature changes caused by downward radiation flux anomalies of SWIN and LWDN.

## 5. RESULTS AND DISCUSSION

These results can be compared to the results calculated by Hansen et al. [34] and Soden et al. [35] who have used complicated GCMs in their analyses. In these models the temperature effects are based on the eruption aerosol amounts and properties. When comparing the dynamic behavior, the calculated  $T_m$  of GCMs follows very accurately the real temperature change as does the **DM**. The conclusion is that the dynamical time delays in their GCMs must come very close to the time constants applied in this study.

The peak values of  $T_m$  of the GCM studies are  $-0.6 \text{ }^{\circ}\text{C}$  [34] and  $-0.7 \text{ }^{\circ}\text{C}$  [35] and according to their graphs, the model-predicted values are practically same as the observed values. The observed values of this study vary from  $-0.5 \text{ }^{\circ}\text{C}$  to  $-0.6 \text{ }^{\circ}\text{C}$  based on the selected temperature measurement. One explanation could be that in the referred GCM studies the modified UAH MSU dataset has been used having a greater ENSO effect correction than in this study.

In the GCM calculations the researchers [34]-[35] have used ERBS flux values. In both cases the maximum value of SW anomaly  $\Delta SWIN$  has been about  $-4 \text{ Wm}^{-2}$ , which differs 33 % from the value of  $-6 \text{ Wm}^{-2}$  used in the majority of the other GCM studies and also in this study. The maximum LW anomaly  $\Delta LWUP$  used in the GCM studies has been about  $-2.3 \text{ Wm}^{-2}$ . Using equation (1) for steady-state conditions, the calculated peak  $T_m$  would be  $0.5 \cdot (-4 + 2.3) = -0.85 \text{ }^{\circ}\text{C}$ . This value is very close to the model-predicted value of Soden et al.

[35]. On the other hand, if the commonly used value of  $-6 \text{ Wm}^{-2}$  would have been used, the calculated peak  $T_m$  would be  $0.5 * (-6 + 2.3) = -1.85 \text{ }^{\circ}\text{C}$ . If the average  $\lambda$ -value of  $1.0 \text{ K/(Wm}^{-2})$  commonly found in GCMs is used, the  $T_m$  would be even larger. The GCM simulations of Soden et al. [35] gave results which are close to the measured  $\Delta T$  values. The major features of these two studies are listed in Table 2.

554

555 **Table 2. Comparison of the major differences between the study of Soden et al. [35]**  
556 **and this study**

557

	Soden et al.	Ollila
Min. $\Delta\text{SWIN}$ , $\text{Wm}^{-2}$ , min.	-4.0	-6.0
Max. $\Delta\text{LWDN}$ , $\text{Wm}^{-2}$ , max.	+2.3	+3.6
Max. radiative forcing, $\text{Wm}^{-2}$	-1.7	-2.4
Equil. $T_m$ according to $\lambda = 0.5 \text{ K/(Wm}^{-2})$ , $^{\circ}\text{C}$	<b>-0.85 (-0.75)</b>	-1.2 (-1.1)
Equil. $T_m$ according to $\lambda = 0.27 \text{ K/(Wm}^{-2})$ , $^{\circ}\text{C}$	-0.46 (-0.36)	<b>-0.65 (-0.55)</b>

558

559 The model calculated  $T_m$  values are for equilibrium conditions and the values of the real  
560 dynamic conditions are in brackets. The dynamic simulations of this study show that in the  
561 dynamic change condition the real equilibrium  $T_m$  value cannot be reached but the real  
562 temperature change is about  $+0.1 \text{ }^{\circ}\text{C}$  smaller. The values in Table 2 show that the results of  
563 Soden et al. [35] can be generated using the  $\lambda$  value of  $= 0.5 \text{ K/(Wm}^{-2})$  and the flux values  
564 applied by them.

565

566 This simple analysis shows that the model-predicted  $T_m$  values are completely dependent  
567 on the selected forcing fluxes,  $\lambda$  values and even on the selected observed  $\Delta T$  value. It  
568 appears that in GCM simulations [34]-[35] the selected  $\Delta\text{SWIN}$  flux cannot be regarded as  
569 the justifiable choice. Actually the greatest uncertainty is about the right  $\Delta\text{LWDN}$  flux values,  
570 because there are no direct measurements available. The commonly used  $\Delta\text{LWUP}$  flux at  
571 the TOA, is not the same flux as  $\Delta\text{LWDN}$ .  $\Delta\text{LWUP}$  is mainly dependent on the real RF  
572 fluxes ( $\Delta\text{SWIN}$  and  $\Delta\text{LWDN}$ ) and on the surface temperature. Therefore the  $\Delta\text{LWUP}$  flux  
573 contains the dynamic delays of the land and ocean and the warming/cooling effects of the  
574 forcing radiation fluxes. In the dynamic simulations this is a source of error. The real  
575 measured  $\Delta\text{LWUP}$  fluxes are very spiky – especially ISCCP fluxes.

576

## 577 4. CONCLUSION

578

579 The results show that a simple one dimensional dynamic model **DM** gives results that are  
580 close to the real surface temperature changes  $\Delta T$  after the Mount Pinatubo eruption using  
581 the climate sensitivity parameter value of  $0.27 \text{ K/(Wm}^2)$ . Timewise the changes follow very  
582 well the real changes. It means that the applied time constants for land (1.04 months) and  
583 for ocean (2.74 months) are accurate and can be used in any dynamic simulations.  
584 Especially the quick and large  $\Delta T$  during the early phase of the eruption shows that the  
585 applied **DM** follows very accurately the real change rate.

586

587 The maximum temperature decrease differs  $+0.05 \text{ }^{\circ}$  from the lowest dataset value (UAH  
588 MSU) and  $-0.04 \text{ }^{\circ}\text{C}$  from the highest dataset value (T average) being actually in the middle of  
589 the dataset changes. This is a very good accuracy.

590

591 The climate sensitivity parameter value of  $0.5 \text{ K/(Wm}^2)$  gives the minimum peak value of  
592  $-1.02 \text{ }^{\circ}\text{C}$ , which is almost double in comparison to  $-0.55 \text{ }^{\circ}\text{C}$  calculated by  $\lambda$  value of  $0.27$   
593  $\text{K/(Wm}^2)$ . This means that the climate models are very sensitive to the value of the climate  
594 sensitivity parameter. The mean  $\lambda$ -value of  $1.0 \text{ K/(Wm}^{-2})$  commonly used in GCMs would  
595 give 200 % too high values.

In this study  $\Delta$ SWIN and  $\Delta$ LWDN fluxes have also been estimated utilizing the apparent transmission measurements. The simulation using these fluxes gives the best and consistent results. The theoretical feedback simulation gives values which are close to the DM model values applying also the  $\Delta$ LWDN flux values.

The correlation analysis between the model calculated  $T_m$  and the measured  $T_{av-e}$  gave the correlation  $r_2 = 0.6$  and the standard error of  $T_m = 0.066$  °C. When the standard error of  $T_m$  is transformed into the standard error of  $\lambda$ , the value is  $0.036$  K/(Wm<sup>-2</sup>). This means that the uncertainty of  $\lambda$  is in the range from  $0.234$  K/(Wm<sup>-2</sup>) to  $0.306$  K/(Wm<sup>-2</sup>). The main reason for the relatively poor correlation seems to be the inaccurate surface temperature measurements. The correlation  $r_2$  between  $T_{msu-e}$  and  $T_{av-s}$  is  $0.85$  and the standard error of the estimate  $0.040$  °C. This error is 61 % of the standard error of the DM predicted temperature. If the 7 months running mean is applied to  $T_m$  and  $T_{av-e}$  like in the study of [35],  $r_2 = 0.76$  and the uncertainty range of  $\lambda$  improves from  $0.245$  to  $0.295$ .

The theoretical simulation of negative feedback of the climate system gives  $T_m$  results, which follow well both the DM results and the real  $\Delta T$  measurements.

## 6. COMPETING INTERESTS

The author declares that there are no competing interests existing.

## REFERENCES

1. Russel PB, Livingston JM, Pueschel RF, Bauman JJ, Pollack JB, Brooks SL, et al. Global to microscale evolution of the Pinatubo volcanic aerosol derived from diverse measurements and analyses. *Journal of Geophysical Research*. 1996;101:18745-18763.
2. Gu L, Baldocchi DD, Wofsy SC, Munger JW, Michalsky JJ, Urbanski SP, Boden TA. Response of a deciduous forest to the Mount Pinatubo eruption. *Science*. 2003;299:2035-2038.
3. Farquhar GD, Roderick ML. Pinatubo, diffuse light and the carbon cycle. *Science*. 2003;299:1997-1998.
4. Stowe LL, Carey RM, Pellegrino PP. Monitoring the Mount Pinatubo aerosol layer with NOAA-11 AVHRR Data. *Geophysical Research Letters*. 1992;19:159-162.
5. UAH MSU temperature dataset. <http://www.nsstc.uah.edu/data/msu/>
6. Apparent transmission dataset at Mauna Loa. Available: [http://www.esrl.noaa.gov/gmd/webdata/grad/mloapt/mlo\\_transmission.dat](http://www.esrl.noaa.gov/gmd/webdata/grad/mloapt/mlo_transmission.dat)
7. Wild M, Gilgen H, Roesch A, Ohmura A, Long CN, Dutton EG, et al. From dimming to brightening: decadal changes in solar radiation at Earth's surface. *Science*. 2005;308:847-850.
8. Thomas MA. Simulation of the climate impact of Mt. Pinatubo eruption using ECHAM5. Dissertation at Hamburg University 2008.
9. Minnis P, Harrison EF, Stowe LL, Gibson GG, Denn FM, Doelling DR, Smith WL. Radiative climate forcing by the Mount Pinatubo eruption. *Science*. 1993;259:1411-1415.
10. Raschke E, Kinne S, Stackhouse PW. GEWEX Radiative Flux Assessment (RFA). December 2012, WCRP Report No. 19/2012.
11. Ollila A. Earth's energy balance for clear, cloudy and all-sky conditions. *Development in Earth Science*. 2013;1:September.
12. Ollila A. Dynamics between clear, cloudy and all-sky conditions: cloud forcing effects. *Journal of Chemical, Biological and Physical Sciences*. 2013;4:557-575.
13. Stenchikov GL, Kirchner I, Robock A, Graf H-F, Antuna JC, Grainer RG, et al. Radiative forcing from the 1991 Mount Pinatubo volcanic eruption. *Journal of Geophysical Research*. 1998;103:13837-13857.

- 649 14. Kirchner I, Stenchikov GL, Graf H-F, Robock A, Antuna JC. Climate model simulation of  
650 winter warming and summer cooling following the 1991 Mount Pinatubo volcanic  
651 eruption. *Journal of Geophysical Research*. 1999;104:19039-19055.
- 652 15. Graf H-F, Kirchner A, Robock A, Schyllt I. Pinatubo eruption winter climate effects. Model  
653 versus observations. *Climate Dynamics*. 1993;9:81-93.
- 654 16. IPCC. Climate response to radiative forcing. IPCC Fourth Assessment Report (AR4),  
655 The Physical Science Basis, Contribution of Working Group I to the Fourth Assessment  
656 Report of the Intergovernmental Panel on Climate Change, Cambridge University Press,  
657 Cambridge. 2007.
- 658 17. IPCC. The Physical Science Basis. Working Group I Contribution to the IPCC Fifth  
659 Assessment Report of the Intergovernmental Panel on Climate Change, Cambridge  
660 University Press, Cambridge. 2013.
- 661 18. MODTRAN radiation code. Available: <http://climatemodels.uchicago.edu/modtran/>
- 662 19. Ollila A. The potency of carbon dioxide (CO<sub>2</sub>) as a greenhouse gas. *Development in*  
663 *Earth Science*. 2014;2:20-30.
- 664 20. NOAA. Relative humidity trends. NOAA Earth System Research Laboratory. Available:  
665 <http://www.esrl.noaa.gov/gmd/aggi/>.
- 666 21. Held IM, Soden BJ. Water vapor feedback and global warming. *Annual Review of*  
667 *Energy and Environment*. 2000;25:441-475.
- 668 22. Aldrin M, Holden M, Guttorp P, Bieltvedt Skeie R, Myhre G, Koren Berntsen GT.  
669 Bayesian estimation on climate sensitivity based on a simple climate model fitted to  
670 observations of hemispheric temperature and global ocean heat content. *Environmetrics*.  
671 2012;23: 253-271.
- 672 23. Bengtson L, Schwartz SE. Determination of a lower bound on earth's climate sensitivity.  
673 *Tellus B*. 2012. <http://dx.doi.org/10.3402/tellub.v65i0.21533>
- 674 24. Lewis NJ. An Objective Bayesian Improved Approach for Applying Optimal Fingerprint  
675 Techniques to Estimate Climate Sensitivity. *Journal of Climate*. 2013;26:7414-7429.
- 676 25. Otto A, Otto FEL, Boucher O, Church J, Hegeri G, Piers M, et. al. Energy budget  
677 constraints on climate response. *Nature Geoscience*. 2013;6:415-416.  
678 <http://dx.doi.org/10.1038/ngeo1836>.
- 679 26. Harde, H. Advanced two-layer climate model for the assessment of global warming by  
680 CO<sub>2</sub>. *Open Journal of Atmospheric and Climate Change*. 2014;1:1-50.
- 681 27. Lindzen RS, Yong-Sang C. On the observational determination of climate sensitivity and  
682 its implications. *Asia-Pacific Journal of Atmospheric Sciences*. 2011;47:377-390.
- 683 28. Ramachandran S, Ramaswamy V, Stenchikov GL, Robock A. Radiative impact of the  
684 Mount Pinatubo volcanic eruption: Lower stratospheric response. *Journal of Geophysical*  
685 *Research*. 2000;105:409-424.
- 686 29. Yang F, Schlesinger ME. On the surface and atmospheric temperature changes  
687 following the 1991 Pinatubo volcanic eruption: A GCM study. *Journal of Geophysical*  
688 *Research*. 2002;107:4073.
- 689 30. Forster F, Collins M. Quantifying the water vapour feedback associated with post-  
690 Pinatubo global cooling. *Climate Dynamics*. 2004;23:207-214.
- 691 31. Kelly PM, Jones PD, Pengqun J. The spatial response of the climate system to explosive  
692 volcanic eruptions. *International Journal of Climatology*. 1996;16:537-550.
- 693 32. Hansen J, Lacis A, Ruedy R, Sato M. Potential climate impact of Mount Pinatubo  
694 eruption. *Geophysical Research Letters*. 1992;19:215-218.
- 695 33. Timmreck C, Graf H-F, Kirchner I. A one and a half year interactive MAECHAM4  
696 simulation of Mount Pinatubo aerosol. *Journal of Geophysical Research*. 1999;104:9337-  
697 9359.

- 698 34. Hansen J, Sato M, Ruedy R, Lacis A, Asamoah K, Borenstein S, et al. A Pinatubo  
699 climate modelling investigation. NATO ASI Series. 1996;l:233-272.
- 700 35. Soden BJ, Wetherald RT, Stenchikov GL, Robock A. Global cooling after the eruption of  
701 Mount Pinatubo: A test of climate feedback by water vapor. Science. 2002;296:727-730.
- 702 36. Vonder Haar TH, Bytheway JL, Fortsyth JM. Weather and climate analyses using  
703 improved global water vapor observations. Geophysical Research Letters.  
704 2012;39:L16802, doi:10.1029/2012GL052094.
- 705 37. NVAP dataset. NCEP/NCAR Reanalysis. Available:  
706 <http://www.esrl.noaa.gov/psd/data/timeseries/>
- 707 38. ISCCP radiation fluxes. Available: <http://isccp.giss.nasa.gov/products/products.html>
- 708 39. ERBS radiation fluxes. Available: [https://eosweb.larc.nasa.gov/project/erbe/erbe\\_table](https://eosweb.larc.nasa.gov/project/erbe/erbe_table)
- 709 40. HadCRUT4 temperature dataset. Available:  
710 [https://eosweb.larc.nasa.gov/project/erbe/erbe\\_table](https://eosweb.larc.nasa.gov/project/erbe/erbe_table)
- 711 41. GISS/NASA temperature dataset. Available:  
712 [http://data.giss.nasa.gov/gistemp/tabledata\\_v3/GLB.Ts+dSST.txt](http://data.giss.nasa.gov/gistemp/tabledata_v3/GLB.Ts+dSST.txt)
- 713 42. UAH RSS temperature dataset. Available:  
714 [http://data.remss.com/msu/monthly\\_time\\_series/RSS\\_Monthly\\_MSU\\_AMSU\\_Channel\\_T](http://data.remss.com/msu/monthly_time_series/RSS_Monthly_MSU_AMSU_Channel_T)  
715 [LT\\_Anomalies\\_Land\\_and\\_Ocean\\_v03\\_3.txt](http://data.remss.com/msu/monthly_time_series/RSS_Monthly_MSU_AMSU_Channel_T)
- 716 43. Santer BD, Wigley TML, Doutriaux C, Boyle JS, Hansen JE, Jones PD, et al. Accounting  
717 for the effects of volcanoes and ENSO in comparisons of modelled and observed  
718 temperature trends. Journal of Geophysical Research. 2001;106:28033-28059.
- 719 44. Thompson DWJ, Wallace JM, Jones PD, Kennedy JJ. Identifying signatures of natural  
720 climate variability in time series of global-mean surface temperature: Methodology and  
721 insights. Journal of Climate. 2009;22:6120-6141.
- 722 45. NOAA Oceanic Nina Index – ONI. Available:  
723 [http://www.cpc.ncep.noaa.gov/products/analysis\\_monitoring/ensostuff/ensoyears\\_1971-](http://www.cpc.ncep.noaa.gov/products/analysis_monitoring/ensostuff/ensoyears_1971-)  
724 [2000\\_climo.shtm](http://www.cpc.ncep.noaa.gov/products/analysis_monitoring/ensostuff/ensoyears_1971-)
- 725 46. Stine AR, Huybers P, Fung IY. Changes in the phase of the annual cycle of surface  
726 temperature. Nature. 2009;457:435-441.
- 727 47. Kauppinen J, Heinonen JT, Malmi PJ. Major Portions in Climate Change: Physical  
728 approach. International Review of Physics. 2011;5:260-270.